Journal of Volcanology and Geothermal Research 193 (2010) 171–181

Contents lists available at ScienceDirect

Journal of Volcanology and Geothermal Research

journal homepage: www.elsevier.com/locate/jvolgeores

The regular shape of stratovolcanoes: A DEM-based morphometrical approach

Dávid Karátson [a,*,1], Massimiliano Favalli [b], Simone Tarquini [b], Alessandro Fornaciai [b], Gerhard Wörner [a]

[a] Geoscience Center, University of Göttingen, Goldschmidtsrasse 1, 37077 Göttingen, Germany
[b] Istituto Nazionale di Geofisica e Vulcanologia, via della Faggiola 32, 56126 Pisa, Italy

ARTICLE INFO

Article history:
Received 13 November 2009
Accepted 26 March 2010
Available online 1 April 2010

Keywords:
stratovolcano
SRTM
shape analysis
elevation profile
circularity

ABSTRACT

We studied the shape of the most regular-shaped stratovolcanoes of the world to mathematically define the form of the ideal stratovolcano. Based on the Shuttle Radar Topographic Mission data we selected 19 of the most circular and symmetrical volcanoes, which incidentally all belong to subduction-related arcs surrounding the Pacific. The selection of volcanoes benefitted from the introduction of a new definition of circularity which is more robust than previous definitions, being independent of the erosional dissection of the cone.

Our study on the shape of stratovolcanoes was based on the analysis of the radial elevation profiles of each volcano. The lower half section of the volcanoes is always well fitted by a logarithmic curve, while the upper half section is not, and falls into two groups: it is fitted either by a line ("C-type", conical upper part) or by a parabolic arc ("P-type", parabolic/concave upper part). A quantitative discrimination between these groups is obtained by fitting their upper slope with a linear function: C-type volcanoes show small, whereas P-type volcanoes show significant negative angular coefficient. The proposed threshold between the two groups is -50×10^{-4}°/m.

Chemical composition of eruptive products indicates higher SiO_2 and/or higher H_2O content for C-type volcanoes, which could imply a higher incidence of mildly explosive (e.g. strombolian) eruptions. We propose that this higher explosivity is responsible for forming the constant uppermost slopes by the deposition of ballistic tephra and its subsequent stabilisation at a constant angle. By contrast, P-type volcanoes are characterized by a smaller SiO_2 and H_2O content, which can be responsible for a higher incidence of effusive events and/or a lower incidence of upper flank-forming (i.e. mild) explosive eruptions. Therefore, the concave upper flanks of these volcanoes may be shaped typically by lava flows. Based on this hypothesis, we propose that the morphometric analysis of the elevation profile of stratovolcanoes can provide insights into their dominant eruptive style.

1. Introduction

The remarkably regular shape of stratovolcanoes is exemplified by textbook examples such as Mayon (The Philippines), Egmont (New Zealand), Cotopaxi and Parinacota (North Andes), or Kliuchevskoi (Kamchatka). These volcanoes have been, and still are, referred many times as to "stratocones" implying a conical shape. However, more than a century ago Milne (1878) recognized the shape of stratovolcanoes is better described as "logarithmic". Francis (1993) investigated the problem from the viewpoint of stratovolcano evolution, and for the simplest, regular landform, provided the formula $r = B\times e^{Mh}$ (r is the radius of the volcano base, h is the height of the volcano, and B and M are constants) which, in explicit form for h, is a logarithm. In a summary of composite volcanoes, Davidson and De Silva (2000) discussed the question of shape in a temporal context, and concluded that during growth, a volcano evolves from a primary, conical stage to a mature, "equilibrium" stage. While youthful volcanoes may show conical profiles with constant slopes, the equilibrium profile of the mature volcanoes is characterized by an accentuated concave slope due to the increasingly large clastic apron of the volcano (Cotton, 1952; Francis, 1993; Davidson and De Silva, 2000). However, a quantitative topographic or morphometric analysis and systematic comparison between "stratocones" of different age, setting and average composition has never been attempted.

In this paper we investigate 19 of the most regular and symmetric stratovolcanoes from different regions of the world (Fig. 1). We quantitatively analyze their shapes based on digital elevation model (DEM) to define the precise form of "ideally shaped" stratovolcanoes, linking morphometry to lava composition and eruptive style.

2. Finding the ideal shape

2.1. The input DEM

To carry out a worldwide survey of stratovolcano morphologies we need a global elevation dataset which adequately represents the form

* Corresponding author. Permanent address: Department of Physical Geography, Eötvös University, Pázmány s. 1/c, H-1117 Budapest, Hungary.
E-mail addresses: dkarat@ludens.elte.hu (D. Karátson), favalli@pi.ingv.it (M. Favalli), tarquini@pi.ingv.it (S. Tarquini), fornaciai@pi.ingv.it (A. Fornaciai), gwoerne@gwdg.de (G. Wörner).
[1] Tel.: +49 551 393972; fax: +49 551 393982.

0377-0273/$ – see front matter © 2010 Elsevier B.V. All rights reserved.
doi:10.1016/j.jvolgeores.2010.03.012

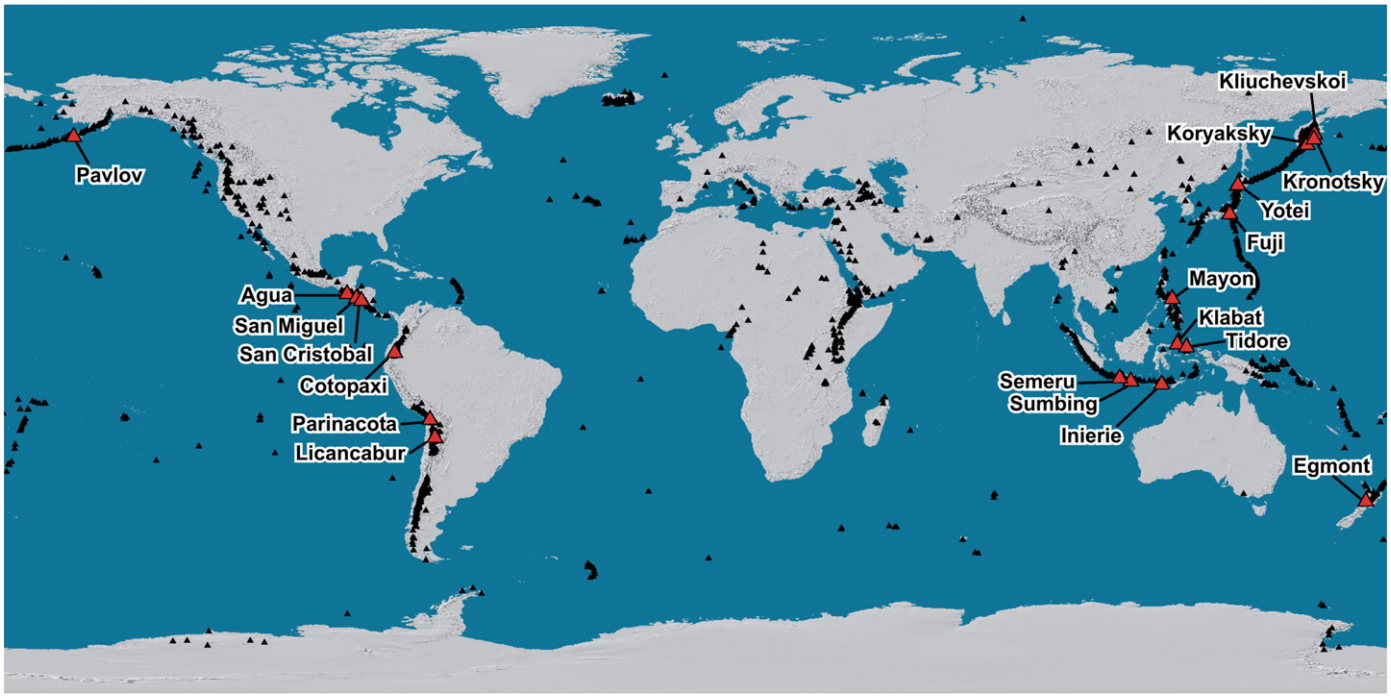

Fig. 1. Location of 19 of the most regular stratovolcanoes of the world, selected by our morphometric analysis.

of volcanoes. At the beginning of this century a quasi-global elevation dataset from the Shuttle Radar Topographic Mission (SRTM) was released (Rabus et al., 2003; Berry et al., 2007; Farr et al., 2007). It consists of a 90 m-cell size DEM which has been shown to be appropriate for volcano morphometry (Wright et al. 2006; Kervyn et al., 2008; Grosse et al., 2009).

The global ASTER DEM with a 30 m-cell size has been released more recently (Hayakawa et al., 2008). However, in spite of its higher nominal resolution, the SRTM DEM warrants an essentially constant quality, while the quality of ASTER DEM is uneven (Crippen et al., 2007; Huggel et al., 2008). This difference is due in part to the wavelengths used by the two systems. The ASTER sensor works in the near infrared bandwidth which is disturbed by clouds coverage, while the SRTM works with microwave frequencies which are not affected by clouds (Stevens et al., 2004; Hubbard et al., 2007). Although the rather low resolution of SRTM DEM cuts off the contribution of short wavelengths to the actual shape, these are not relevant in describing the overall volcano shape, while large-scale features are adequately represented (Wright et al., 2006). For this reason our analysis is based on the SRTM elevation dataset.

2.2. Circularity of stratovolcanoes

It is generally accepted that the ideal stratovolcanoes have a perfect circular symmetry (Francis 1993; Davidson and De Silva, 2000). We analysed this circular symmetry by using the DEM in grid format as well as 50 m-interval elevation contours derived from the DEM. We considered only the closed contour lines around the volcano, discarding the lower contours disturbed by the surrounding morphology.

The circularity index of a shape is a dimensionless number quantifying how much a shape metric (in our case the elevation contour) fits to that of a circle. For a circle, circularity is one and it tends to zero as the shape becomes less and less circular. The most common definition of circularity (c_1) is the ratio of the area of a shape to the area of the circle having the same perimeter of the shape. In fact, c_1 is a measure of the compactness of a shape: the more compact a shape is, the closer c_1 is to unity, the circle representing the most compact shape and hence having c_1 equal to one. Another common definition of circularity (c_2) is given by the ratio of the circumference of the circle having the same area as the shape to the perimeter of the shape itself.

These definitions use the perimeter of the shape and are thus highly dependent on the small-scale noise of the shape. This is misleading when characterizing stratovolcanoes that have an overall circular symmetry but are dissected by small incisions/valleys. Therefore, we introduce a different definition of circularity:

$$c = 1 - \frac{\sigma_{R_i}}{R_i} \tag{1}$$

where R_i is the average radius of the shape boundary calculated with respect to the barycentre of the shape boundary itself, and σ_{R_i} is the standard deviation of the distance of the points of the shape boundary from the average radius R_i. This formula keeps circularity values in the same range of the previous formulation, but provides much more suitable and robust results for our purpose.

For example, Kronotsky volcano, Kamchatka (Fig. 2) has a very high overall circular symmetry, while, at smaller scales, its flanks are highly irregular due to the presence of a great number of gullies. For this reason circularity measures c_1 and c_2 have low values, while the much higher values of c better represent the good overall circular form of the volcano (Fig. 3). On the other hand, the top of the volcano displays elliptical but smooth contours which decreases the overall circularity, hence we will have values of c lower than c_1 and c_2. In contrast, Mayon volcano (The Philippines) has a very good circular shape at all elevations and it is much less dissected, which results in similar values for all the circularity metrics.

To further compare the robustness of the three definitions of circularity, we considered a simplified ultra-dissected cone whose horizontal section, at a given height, has the shape of a circular saw blade profile with a 1 km radius and triangular 60 m-spaced 60 m-height teeth. According to the above definitions of circularities, this section has $c \cong 0.98$, $c_1 \cong 0.2$ and $c_2 \cong 0.45$, while $c = c_1 = c_2 = 1$ for a circle. This result highlights that c is the circularity definition that is by far the least affected by short wavelength perturbations, proving the remarkable robustness of the c values for large-scale shape analysis.

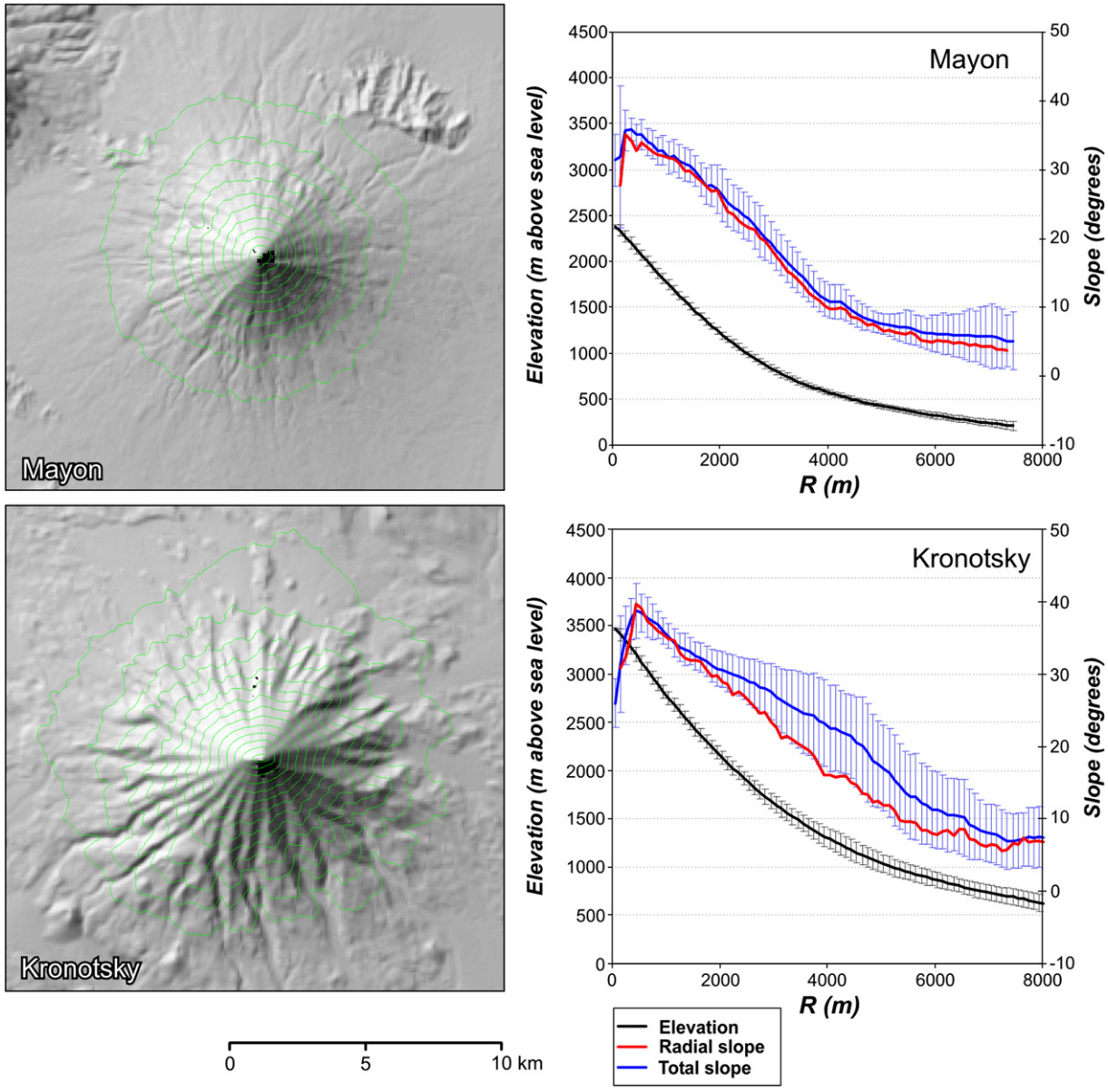

Fig. 2. Shaded relief images of Kronotsky (Kamchatka) and Mayon (The Philippines) volcanoes with 200 m contour lines. Plots highlight the different patterns of the radial and total slopes for the two volcanoes (see text). The error bars of the radial elevation profiles (black) confirm the difference.

For each volcano, we defined its centre of symmetry $\vec{X}_c = (X_c, Y_c)$ as the weighted average of the barycentres of all related closed contour lines:

$$\vec{X}_c = \frac{1}{N}\sum_i \left(\frac{R_i}{\sigma_{R_i}}\right)^4 \vec{X}_{C_i} \tag{2}$$

where $\vec{X}_{C_i}$ is the barycentre and R_i is the average radius of the ith contour line, and σ_{R_i} is the standard deviation of the distances of the points of the ith contour line from the barycentre $\vec{X}_{C_i}$. As possible weight we have checked various positive integers' powers of the ratio R_i/σ_{R_i}. The R_i/σ_{R_i} argument of power law ensures that the more irregular a contour is, the lower influence it has on the determination of the centre. The lowest exponent providing a stable position for $\vec{X}_C$ proved to be the 4th power. N is the normalization factor given by the sum of all the weights: $N = \sum_i \left(R_i/\sigma_{R_i}\right)^4$.

Then, we computed maps of the circular symmetry for each volcano by using their DEM, and considering circles of increasing radius centred on $\vec{X}_C$ (Fig. 4). On every circle the average elevation H_R is computed, and for each point of the circle its deviation σ_c from H_R is expressed. The map of the deviations (Fig. 4) quantifies the circular symmetry of the DEM with respect to $\vec{X}_C$. Outwards, the volcano profiles merge with the surrounding terrain. To include the outermost portion of the profiles, for some volcanoes we expanded the boundary of the maps outwards along selected directions not disturbed by extraneous features.

2.3. Selecting the most regular stratovolcanoes

We downloaded the Earth's active volcanoes' database from the Smithsonian Institute website to have a guidance in carrying out a systematic approach. By visually surveying shaded relief images on SRTM DEM, we selected about eighty regular-shaped volcanoes. The selection has been made as an elicitation process involving all co-authors. The selection criteria were symmetry, significant size, and an apparent simple cone shape; therefore, both subduction-related and intraplate volcanoes have been selected. Subsequently, for each volcano

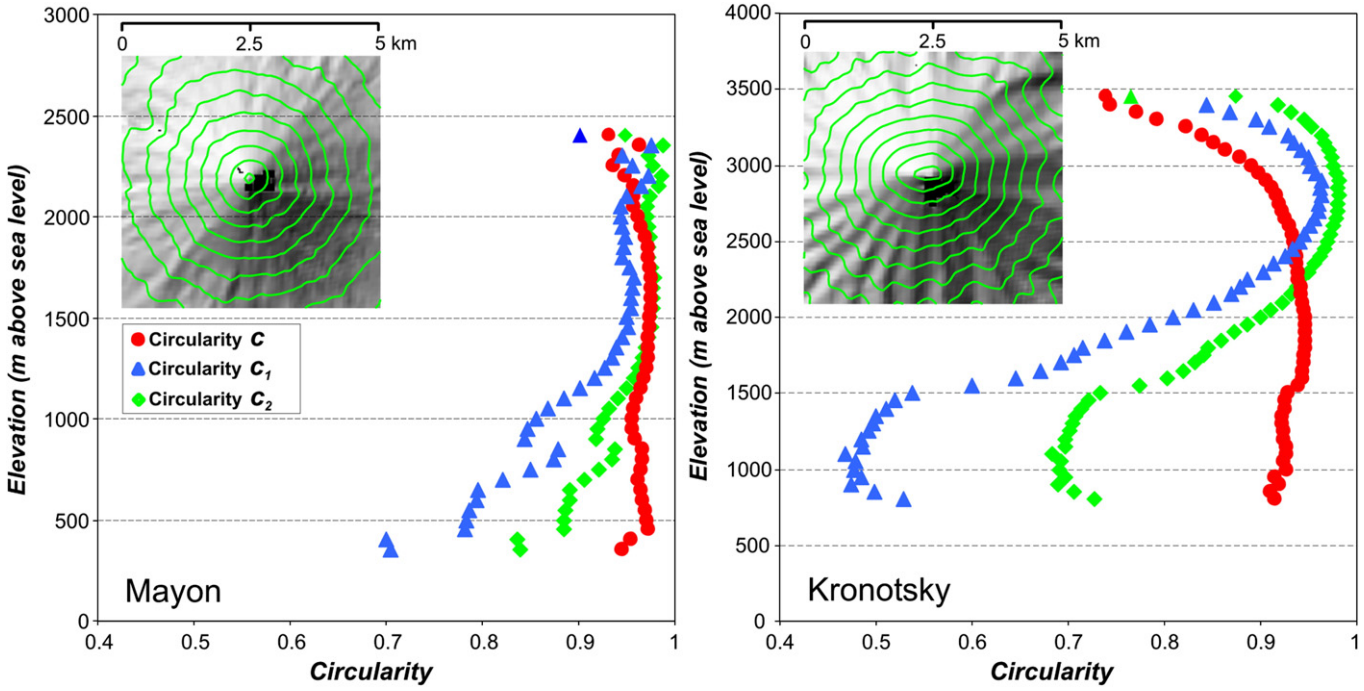

Fig. 3. Circularity (c, c_1 and c_2, see text for definitions) versus elevation plots for Mayon and Kronotsky volcanoes. Insets show the top of the volcanoes with 200 m contour lines. Kronotsky has an elliptical summit, while Mayon keeps very good circularity values up to the top.

we computed maps of circular symmetry, and circularity values relative to the centre of symmetry. To get rid of minor irregularities, we defined c_m as the average of the highest 70% circularity values (hence cutting off the lower 30%). We discarded the less symmetric volcanoes based on the maps of circular symmetry and using a subjective limit in c_m values (c_m<0.9). Our final selection includes 19 volcanoes (Fig. 1, Table 1). This approach excludes older stratovolcanoes (>~100 kyr) and/or those erupting evolved magmas (>~60% SiO_2) as well as volcanoes that have suffered major sector collapse or explosive caldera-forming eruptions during their lifetime.

The final selection includes only subduction-related volcanoes representing different arc segments of the circum-Pacific rim: Kamchatka (hosting the most circular volcano of the world, Kliuchevskoi, c_m = 0.97), the Kuril and Aleutian islands, Central America, Andes, New Zealand, Indonesia, The Philippines, and Japan (Table 1). This sampling covers a range of volcano sizes and very different climatic conditions, including examples from both microcontinental arcs (9) and continental margins (10). We note that not a single intraplate (rift-related or ocean-island type) stratovolcano has passed our morphometric sieve. The highly symmetric initial shape of youthful continental-margin stratovolcanoes can be due to high eruption rates from a central vent, which is later destroyed by morphologic complications during evolution (e.g. twin and compound volcanoes: Francis, 1993; Grosse et al., 2009). The high circular symmetry of the selected stratovolcanoes ensures that their morphology is essentially due to the growth of a single, central volcano, not influenced by the neighboring volcanic systems, tectonic movements or asymmetric erosion (e.g. by glaciers). Our selection also excludes volcanoes which are known to have grown on inclined landscapes, such as Arenal (see Fig. 4 in Borgia and Linneman, 1990).

3. Elevation and slope profile analysis

For each volcano, we calculated the average radial profile by averaging the elevation of all the points at the same distance R from the centre $\vec{X_C}$ (Fig. 5). We started our analysis from a radius of about 300 m. Considering the 90 m-cell size of SRTM DEM, a point of the average radial profile at R = 300 m has an elevation which is the average of the elevation values of about 20 cells laying on the circle with R = 300 m. If we exclude that the errors in our DEMs are systematically correlated to the distance from our centre of circular symmetry (which is likely the truth), then any other error in the DEM is drastically reduced in the average radial elevation profile by averaging a large number of elevation values. Being the SRTM dataset assessed for large-scale morphology of volcanoes, we conclude that the effect of DEM errors on our analysis is negligible.

From the radial profile we obtained the average radial slope profile as a function of R. It must be stressed that this slope profile does not account for the component of the elevation gradient which is not arranged along the radius: if we plot the average radial slope and the total slope (i.e. including non-radial components) against the radial distance from the centre of symmetry $\vec{X_C}$, the difference between these two slopes will represent the contribution of dissection to the total slope (Fig. 3).

3.1. The lower part of the profiles

In agreement with the literature, we found that the lower parts of all the studied stratovolcano profiles are always well fitted by a logarithmic curve:

$$\tilde{H} = \log \tilde{R} \tag{3}$$

where $\tilde{R}=\alpha(R-R_0)$ and $\tilde{H}=\beta(H-H_0)$, with α, β, R_0 and H_0 constants determined for each volcano. We explored the fit of the lower part of the profiles with respect to other functions of the form of $H=H(R)$, like hyperbolic, exponential and Gaussian functions. These functions provided worse results compared to the log function, the last being the only one that well reproduces the typical (hyperbolic) slope trend in the lower part of the profiles (Fig. 5). Root mean squared (RMS) deviations of the log fits from the actual lower profiles are listed in Table 1. All the RMS deviations are less than 50 m including the strikingly low value of 1.2 m for Mayon.

3.2. The upper part of the profiles

The lower part of the profiles ends where the logarithmic curve stops to fit. We define this change as the starting point of the upper part of the profile, which in turn ends near the summit crater where

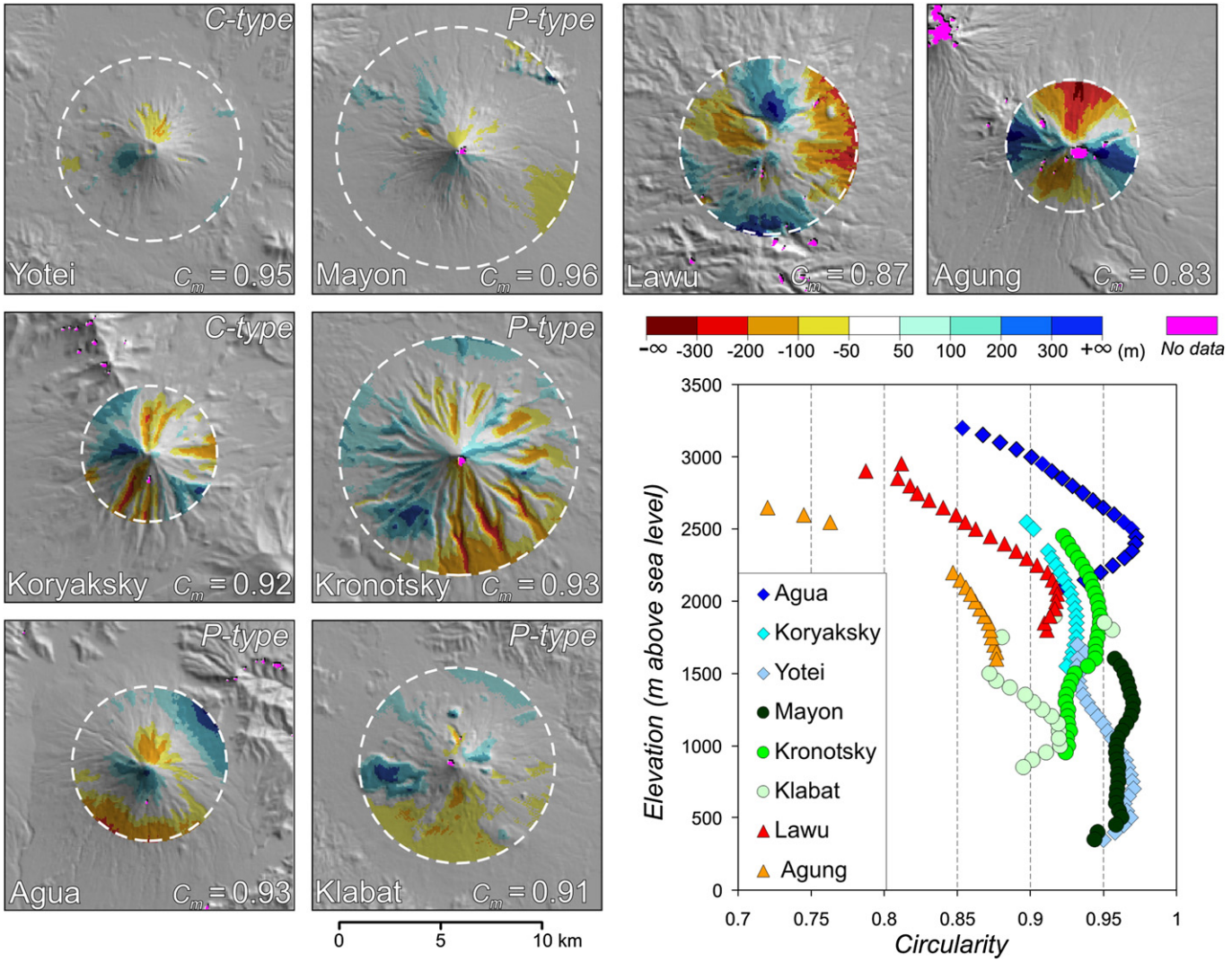

Fig. 4. Maps of circular symmetry and circularity plots for selected stratovolcanoes. For each volcano the average circularity c_m is reported as well as its morphometric type. Yotei and Mayon are perfectly regular textbook volcanoes. Koryaksky and Kronotsky have very good circularity values, despite their flanks are heavily dissected. Lawu and Agung (Indonesia) are examples showing low circularity values for which they were discarded from profile analysis: Lawu is an example of an irregular-shaped form, while Agung has an elliptical shape. For each volcano, the plots shows how the circularity (calculated for closed contours relative to the centre of the symmetry) varies with elevation.

the slope starts to decrease. Whilst the lower profile is always logarithmic, the upper profiles of the studied volcanoes are not all fitted by a single function, but are rather scattered between two end-member functions: a line (actually a conical shape) and a parabola (concave shape: Figs. 5 and 6). On the basis of the affinity to one of the two end-members, we split the studied volcanoes into two morphometric groups, termed C-type (conical) volcanoes (8) and P-type (parabolic) volcanoes (11).

The two groups show largely different upper profiles (the upper ~1000 m on the average; Figs. 6 and 7). In order to discriminate between these types on a quantitative basis, we checked how their slopes can be fitted by a linear function. Whereas C-type volcanoes tend to have a constant slope and are therefore well fitted by a constant function, P-type volcanoes show a constant increase in their slope as the radius decreases, and are fitted by a line with a marked negative angular coefficient (ac). Although both groups show some scatter (Table 1), there is a threshold in between: if $ac > -50\times10^{-4}$°/m we classify the volcano as belonging to C-type (ideally, with $ac=0$), while if $ac < -50\times10^{-4}$°/m we classify it P-type (Table 1).

Furthermore, the average slope at the starting point of the upper profile is 26.7 ± 3.6° for C-type and 21.3 ± 4.4° for P-type. The average slope of the whole upper profile is approximately 30° in both types; it is closer to the angle of repose of scoria cones (~30–31°, Wood, 1980) in C-type (30.3 ± 1.0°) than in P-type (27.7 ± 2.8°). On the other hand, average maximum slopes of the two types are almost identical (33.3 ± 0.7° and 34.2 ± 3.1°). These latter similarities emphasize the fact that we are discussing relatively minor differences in volcano shape.

4. Discussion

We start the discussion with further highlighting the robustness of our measurements with respect to secondary factors which could be supposed to affect the DEMs of the selected volcanoes, and hence the obtained morphometric results. Being geographically scattered between low and high latitudes, the selected volcanoes are exposed to different climates, implying a marked difference in the occurrence of snow/ice cover. A snow/ice coverage will likely smooth the existing topography, nevertheless the robustness of our improved circularity (Section 2.2) minimizes the impact on c values. Similarly, a possible flattening due to snow/ice crater filling will not misplace the bounds of the upper portion of the volcano shape.

Another issue is whether erosional processes in general play a role discriminating between the volcanoes. We already demonstrated that our circularity definition is not affected by the influence of radial

Table 1
Morphometry of selected stratovolcanoes with most important geochemical data. P = Pleistocene, H = Holocene. For discussion of all values see text.

Volcano						Morphometry							Geochemistry			
Name	Location	Latitude (°)	Longitude (°)	Oldest age	Last eruption (yr)	Circularity $1-\sigma_R/R_i$	Max. slope (°)	Average upper slope (°)	Slope at end of log section (°)	Rel. height of upper part (m)	RMS deviation of log fit (m)	Angle variation rate (10^{-4}°/m)	Number of analyses	Range in SiO_2	Molar MgO/($Mg+FeO_{tot}$)	References to geochemical data
Group C																
Semeru	East Java (Indonesia)	−8.108	112.920	?	2010 AD	0.93	33.5	30.6	29.2	1418	34.6	−3	7	56.3–58.4	35.9–37.1	Whitford (1975) and Carn and Pyle (2001)
Inierie	Flores (Indonesia)	−8.587	120.728	H?	8050 BC	0.94	32.9	31.8	30.2	662	15.7	2	7	51.3–58.6	44.8–56.6	Stolz et al. (1990) and Wheller et al. (1987)
Koryaksky	Kamchatka (Russia)	53.320	158.688	Late P	2009 AD	0.92	32.9	29.6	27.3	1447	29.8	−37	7	50.1–59.0	58.0–65.2	Popolitov and Volynets (1981), Kepezhinskas et al. (1997), Bindeman et al. (2004) and Hochstaedter et al. (1996)
Kliuchevskoi	Kamchatka (Russia)	56.057	160.638	6000 BP	2010 AD	0.97	34.4	29.7	19.3	2152	43.3	−37	73	47.7–54.4	48.6–70.6	Dorendorf et al. (2000), Kersting and Arculus (1994) and Portnyagin et al. (2007)
Yōtei	Hokkaido (Japan)	42.830	140.815	<0.1 Ma	5–6 ka BP	0.95	32.0	30.3	23.6	931	5.9	−46	24	54.0–64.6	29.5–40.7	Katsui et al. (1978), Masuda (1979) and Nakagawa (1992)
Licancabur	Central Andes (Chile/Bolivia)	−22.830	−67.880	<10 ka	H	0.94	33.7	31.7	28.4	919	47.7	−35	13	56.8–61.0	44.9–50.6	Figueroa et al. (2009) and Mamani et al. (2009)
Parinacota	Central Andes (Chile/Bolivia)	−18.170	−69.150	< 8 ka	290	0.94	33.2	29.7	27.0	881	9.3	−38	41	57.5–59.1	36.5–49.0	Clavero et al. (2002), Hora et al. (2009) and Wörner et al. (1988, 2000)
Cotopaxi	Northern Andes (Ecuador)	−0.677	−78.436	7.2 ka	1877	0.95	33.8	29.2	28.6	769	4.3	−42	43	56.6–62.8	37.3–59.4	Garrison et al. (2006, personal communication)
Average						0.94	33.3	30.3	26.7	1147	23.8	−29				
Std. dev.						0.02	0.7	1.0	3.6	454	17.2	18				
Group P																
Tidore	Eastern Indonesia	−0.658	127.400	H?	H	0.96	33.0	31.0	27.2	974	18.4	−58	4	54.4–61.7	36.6–47.5	Morris et al. (1983)
Sumbing	Java (Indonesia)	−7.384	110.070	H?	1730	0.95	32.6	28.5	25.1	919	13.5	−60	3	52.2–55.3	53.7	Nicholls and Whitford (1976) and Whitford (1975)
Sundoro	Java (Indonesia)	−7.300	109.992	H?	1971	0.94	33.9	29.5	24.0	923	16.4	−77	3	50.7–54.9	48.1	Nicholls and Whitford (1976) and Whitford (1975)
Klabat	Sulawesi (Indonesia)	1.470	125.030	H	Fumarolic	0.91	31.6	25.5	21.9	829	4.3	−74	1	57.1	45.3	Morrice et al. (1983)
Mayon	Philippines	13.257	123.685	Late P	2009	0.96	35.1	28.1	19.7	1545	1.2	−61	24	52.0–57.0	47.9–53.4	Castillo and Newhall (2004)
Kronotsky	Kamchatka (Russia)	54.753	160.527	Late P	1923	0.93	39.6	29.3	19.5	2062	29.9	−61	2	50.5–52.5	43.7–50.1	Popolitov and Volynets 1981 and Tolstikhin et al. (1974)
Agua	Guatemala	14.465	−90.743	H?	H	0.93	37.5	31.6	26.1	1550	40.4	−54	24	52.3–59.8	39.0–49.9	Cameron et al. (2002)
San Miguel	El Salvador	13.434	−88.269	H?	2002	0.96	30.6	22.7	13.3	1465	14.0	−63	5	49.7–51.9	43.1–47.0	Carr (1984), Carr et al. (1981), Leeman et al. (1994) and Agostini et al. (2006)
San Cristóbal	Nicaragua	12.702	−87.004	H?	2009	0.93	30.2	24.9	15.4	994	7.2	−91	3	49.0–51.3	49.5	Carr (1984) and Leeman et al. (1994)
Pavlof	Alaska	55.420	−161.887	<10 ka	2007	0.96	38.2	29.0	23.0	1255	20.5	−89	5	51.4–53.5	42.1–48.1	McNutt et al. (1991)
Egmont	New Zealand	−39.300	174.070	<8 ka	1854	0.91	34.4	25.0	19.3	1237	20.7	−62	24	49.5–59.4	37.3–48.4	Neall et al. (1986) and Stewart et al. (1996)
Average						0.94	34.2	27.7	21.3	1250	17.0	−68				
Std. dev.						0.02	3.1	2.8	4.4	377	11.3	12.7				

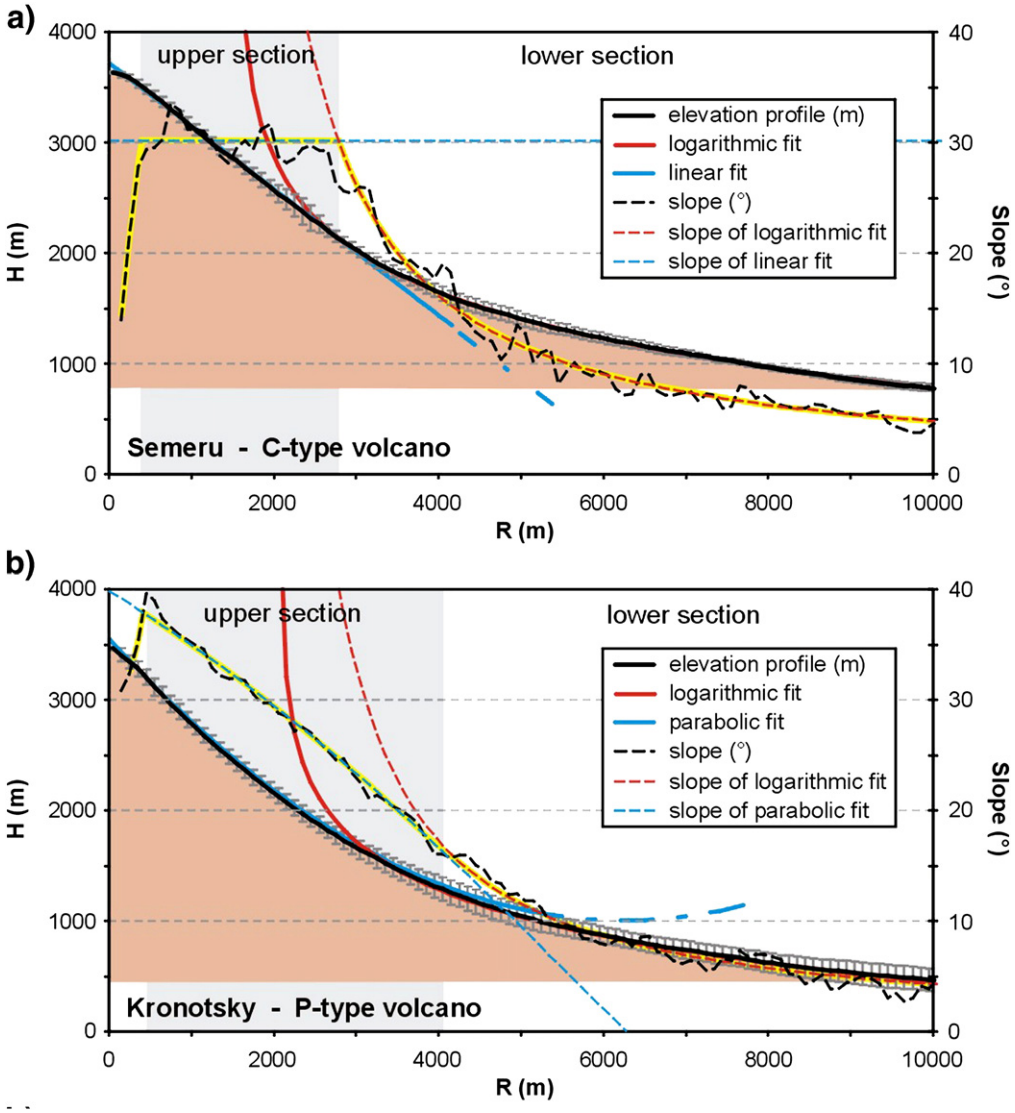

Fig. 5. Examples of average radial elevation and slope profiles: a) Semeru for group C; b) Kronotsky for group P. Thick solid lines represent profiles and fitted curves, while thin dashed lines are their slopes. The lower flanks of both volcanoes are fitted well by logarithmic curves, while the upper part (shaded) is fitted by a line (i.e. conical shape) for Semeru (C-type volcano) and by a parabolic curve for Kronotsky (P-type volcano). The yellow lines highlight the slope of the ideal C- and P-type profile.

dissection. However, we should also address if erosional processes act on the whole surface. Because some of our selected volcanoes have extincted a long time ago (having Early Holocene last eruptions), the high erosion rates on active to dormant volcanoes (up to 1000 mm/ka, depending on climate: e.g. Ruxton and McDougall 1967; Ollier and Brown 1971; Drake 1976; Ollier 1988) can be supposed to modify the regular shape. On the contrary, it is well known that, on fresh cones, erosion does not touch the whole surface, but operates generally through a developing gully system, called parasol ribbing (Cotton, 1952; Francis, 1993; Karátson et al., 1999; Davidson and De Silva, 2000). This initial erosion leaves the original surfaces intact between the deeply-cut ravines for a long time. That the overall shape is not modified is also supported by the obtained angle variation rates of the upper slopes: volcanoes with recent activity and with Holocene activity have the same or very similar values. For instance, in type C, Inierie volcano, last erupted 8050 BC, has as perfect profile as the active Semeru; the 5–6 ka old Yotei has poorer shape but it has the same angle variation rate as the active Kamchatkan volcanoes and Cotopaxi (with an 1877 last eruption). Similarly, in type P, the Holocene Klabat and Agua volcanoes have the same angle variation rates as several others having recent or active status. So, because slope profile and volcano age do not correlate, the erosion during the short time after extinction makes no difference.

As seen above, the radial elevation profiles of both types can be divided into two. The lower part, well fitted by a logarithm, corresponds to the apron of the volcano, and is the result of the combined action of deposition from primary pyroclastic flows and falls to syn- and post-eruptive re-working (e.g. Davidson and De Silva, 2000). These processes surely have different incidence on our volcanoes, but the result is always a general logarithmic law. An exponential thinning law for tephra fallout was already pointed out (Pyle, 1989), but none of the primary and secondary mass transfer processes on the slopes are known or expected to produce deposits with a logarithmic thinning. We infer then that the logarithmic equilibrium curve derives from a combination of different volcano-related mass transport processes on the lower flanks.

The more different upper part of the elevation profiles corresponds to the central zone of the volcanic edifice that may reflect a specific stratovolcano growth pattern. Differences in the elevation profiles between C and P type volcanoes should therefore be related to near-vent and upper slope processes, corresponding to differences in eruptive style, eruptive products and/or erosive processes.

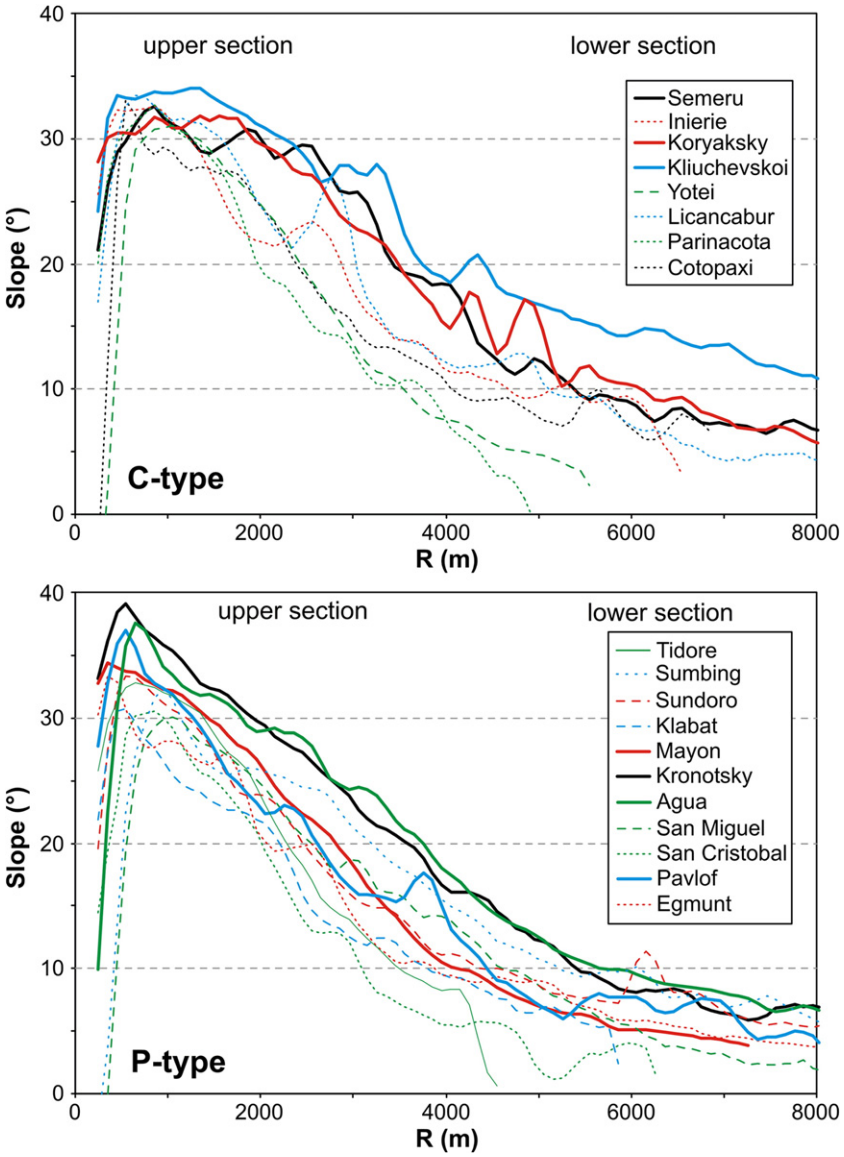

Fig. 6. Smoothed slope profiles of the two morphometric groups.

Consequently, we focus our further discussion on the eruptive behaviour and formation of the upper cone. The near-vent upper slopes of stratovolcanoes are largely dominated by the emplacement of short lava flows in addition to minor tephra deposits, e.g. ballistic ejecta (e.g. Williams and McBirney, 1979; Borgia et al., 1988; McKnight and Williams, 1997; Davidson and De Silva, 2000; Lyons et al., 2009). Proportion of lavas vs tephra is determined by explosivity, which in turn is controlled by the composition of magma. Hence, geochemistry of erupted rocks should be considered.

Chemical analyses of volcanic products are unevenly available for our selected volcanoes, nevertheless, we carried out a detailed survey of the available literature (Table 1). In addition to the cited references, the GEOROC database (Geochemistry of Rocks of the Oceans and Continents, Max-Planck-Institut für Chemie in Mainz, Germany, http://georoc.mpch-mainz.gwdg.de) has been used.

Explosivity vs effusivity is determined by the SiO_2 and H_2O content of magma prior to eruption which both control viscosity. Since the concentration of volatiles increases with melt differentiation (increasing SiO_2 and decreasing MgO content), we plotted the collected data in the SiO_2 vs molar $MgO/(MgO + FeO_{tot})$ diagram (Fig. 8).

Obviously, there is no simple relationship between major element composition, i.e. degree of magmatic differentiation, and stratovolcano shape. However, we recall that our analysis is restricted to highly symmetric cones, hence volcanoes with longer eruptive histories and magmatic differentiations were excluded. As a result of our selection, the cones considered here are all rather mafic in composition. This similarity well explains their small variations in morphology. However, we propose that minor systematic differences do exist.

As seen in Fig. 8, C-type volcanoes, in general, fall either on the more mafic (e.g. two Kamchatkan volcanoes) or on the more differentiated (best represented by the large Andean stratovolcanoes) field of the compositional range. As for the latter, higher silica contents due to slightly more differentiated compositions are typical for Andean magmas since these ascend, cool and differentiate during their passage through a thick crust (e.g. Hora et al., 2009). This process will also result in higher water content as well as higher magma viscosity that may be responsible for higher explosivity (i.e. andesites/dacites of C-type volcanoes). Kliuchevskoi and other C-type stratovolcanoes from the Kamchatka peninsula, in contrast, are more mafic (higher MgO value) and less silicic. However, Kliuchevskoi and Koryatsky volcanoes are also

Fig. 7. Representative profiles of C- and P-type volcanoes. Parinacota and Licancabur (both in Central Andes, Chile, photo by D. Karátson) are characterized by constant upper slopes, i.e. their upper part is conical; Kronotsky (Kamchatka, Russia, credit: Andrey Bogdanov) and Mayon (Luzon, the Philippines, credit: Alastair Robinson) have concave upper slopes, best fitted by a parabola.

known to be highly explosive, and to erupt arc basaltic magmas with high water content (Sobolev and Chaussidon, 1996). Both occur in a region that may have an unusual water-rich mantle source related to the subduction of the Emperor seamount chain (Dorendorf et al., 2000; Auer et al., 2009). High water content, therefore, is the main factor of that they belong to C-type volcanoes. At the same time, the third, highly symmetric

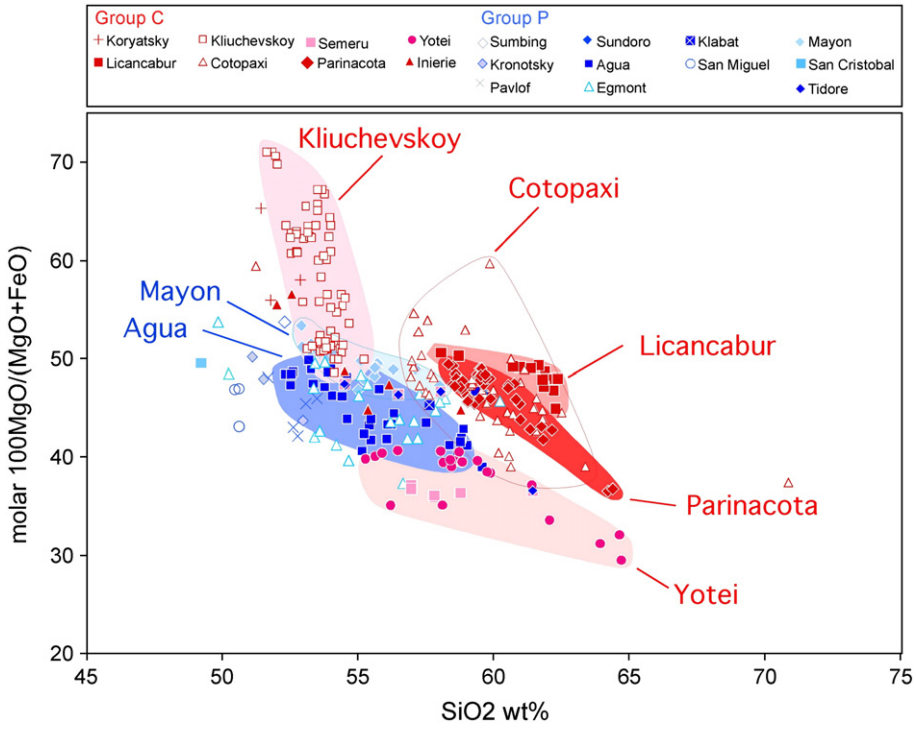

Fig. 8. SiO_2 vs molar MgO/(MgO + FeO) plot for the studied 19 stratovolcanoes. For discussion, see text.

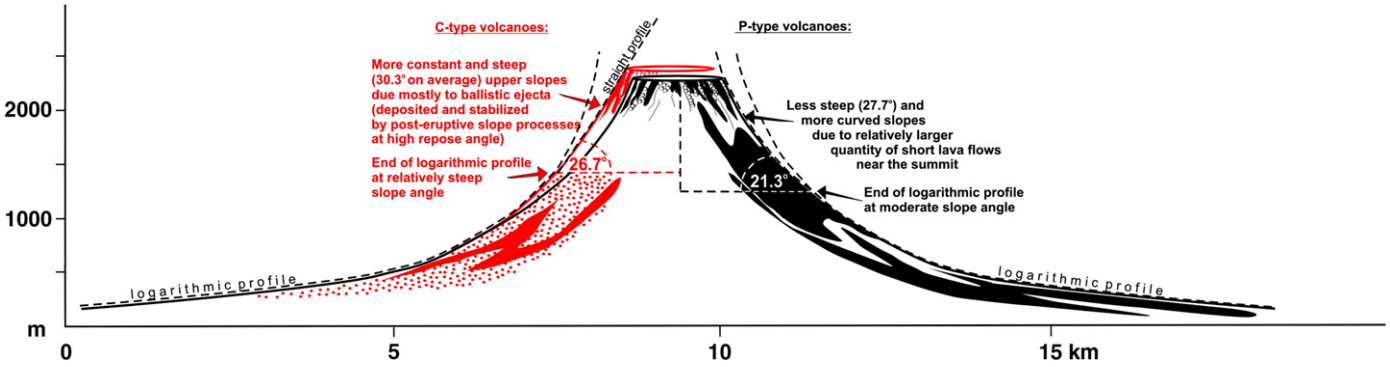

Fig. 9. General interpretative sketch highlighting the main characteristics of the proposed two types of stratovolcanoes.

(although dissected) Kamchatkan volcano, Kronotsky, falls into P type. We think that its eruptive style or rate may have changed relative to the others, modifying its profile without destroying the circular symmetry.

In summary, we propose (Fig. 9) that the summit of type C volcanoes should grow, in addition to short lava flows, by a high frequency of typically mildly explosive (i.e. strombolian, ultra-strombolian) eruptions. The constant upper slope of these volcanoes is similar to the profiles of scoria cones (~30–31°), which may suggest a similar slope construction mechanism, possibly including deposition of fallout and ballistic tephra, occasional welding, and slope creep.

By contrast, P-type volcanoes, as shown by examples from Central America, New Zealand, and parts of Indonesia, may have relatively more mafic and at the same time less water-rich magmas. This compositional difference indicates a higher incidence of effusive activity and/or more scarce mild explosive (e.g. strombolian) eruptions forming the upper slopes of the volcano. This does not mean that these volcanoes — as well as in C-type — cannot have highly explosive eruptions (which however do not form the upper slopes); instead, this compositional difference implies that the frequency of effusive events relative to mild explosive eruptions is bigger than in C-type. Accordingly, we suggest that the upper flanks of P-type volcanoes are more strongly shaped by lava flows than by pyroclastic deposits.

Given the general geomorphic and eruptive similarities between the two stratovolcano types, the two groups do overlap in the long term. We conclude that the composition and eruptive style of these volcanoes, reflected in their morphologies, represent just a snapshot in time, hence all these characteristics may change during stratovolcano evolution, which will result in changing profiles. However, since the slope pattern of the upper flanks may form during a several thousand year-long period, we suggest that the morphometric analysis of the upper slopes of less known stratovolcanoes, especially remote ones where access and field work are difficult, can provide some insights into their dominant eruptive style through time.

5. Conclusions

A detailed analysis of radial elevation profiles of the selected 19 regular-shaped volcanoes revealed that, while the lower section is always well fitted by a logarithmic curve (proposed by many authors), the upper section — typically about half the volcanic edifice — is fitted by two different functions: a line (C-type volcanoes) or a parabola (P-type volcanoes).

By analyzing the available chemistry of eruptive products of the volcanoes, we propose that the detected morphometric difference is affected by eruptive dynamics due to compositional differences of the magmas. Compared to P-type, C-type volcanoes erupt either more silica-rich or more water-rich magmas, or both. Therefore, we argue that the summit of C-type volcanoes is shaped by a relatively higher incidence of mildly explosive (e.g. strombolian) events, while the summit of P-type volcanoes is shaped by a relatively higher incidence of effusive activity.

Given that the upper slope pattern reflects a long-term eruptive activity, we suggest that this morphometrical approach can help the interpretation of the eruptive style of remote or recently inactive volcanoes, where field data can be hardly obtained.

Acknowledgements

The work was funded by a Humboldt Fellowship for Experienced Researchers (3.3-UNG/1115049 STP) to DK, as well as the Dipartimento della Protezione Civile (Italy) in the frame of the 2007–2009 Agreement with Istituto Nazionale di Geofisica e Vulcanologia (INGV). ST was benefitted from the MIUR-FIRB project "Sviluppo di nuove tecnologie per la protezione e difesa del territorio dai rischi naturali (FUMO)", and AF from the MIUR-FIRB project "Piattaforma di ricerca multi-disciplinare su terremoti e vulcani (AIRPLANE)" n. RBPR05B2ZJ. Helpful reviews of David Pyle and Geoff Wadge are acknowledged.

References

Agostini, S., Corti, G., Doglioni, C., Carminati, E., Innocenti, F., Tonarini, S., Manetti, P., Di Vincenzo, G., Montanari, D., 2006. Tectonic and magmatic evolution of the active volcanic front in El Salvador: insight into the Berlín and Ahuachapán geothermal areas. Geothermics 35, 368–408.

Auer, S.L., Bindeman, I.N., Wallace, P.J., Ponomareva, V.V., Portnyagin, M.V., 2009. The origin of hydrous, high-$\delta^{18}O$ voluminous volcanism: diverse oxygen isotope values and high magmatic water contents with the volcanic record of Klyuchevskoy volcano, Kamchatka, Russia. Contrib. Mineral. Petrol. 157, 209–230. doi:10.1007/s00410-00008-00330-00410.

Berry, P.A.M., Garlick, J.D., Smith, R.G., 2007. Near-global validation of the SRTM DEM using satellite radar altimetry. Rem. Sens. Env. 106, 17–27. doi:10.1016/j.rse.2006.07.011.

Bindeman, I., Ponomareva, V.V., Bailey, J.C., Valley, J.W., 2004. Volcanic arc of Kamchatka: a province with high-^{18}O magma sources and large-scale $^{18}O/^{16}O$ depletion of the upper crust. Geochim. Cosmochim. Acta 68, 841–865.

Borgia, A., Linneman, S.R., 1990. On the mechanisms of lava flow emplacement and volcano growth: Arenal, Costa Rica. In: Fink, J.H. (Ed.), Lava Flows and Domes. Emplacement Mechanisms and Hazard Implications: IAVCEI Proceedings in Volcanology, 2. Springer-Verlag, Berlin, pp. 208–243.

Borgia, A., Poore, C., Carr, M.J., Melson, W.G., Alvarado, G.E., 1988. Structural, stratigraphic, and petrologic aspects of the Arenal-Chato volcanic system, Costa Rica: Evolution of a young stratovolcanic complex. Bull. Volcanol. 50, 86–105.

Cameron, B.I., Walker, J.A., Carr, M.J., Patino, L.C., Matias, O., Feigenson, M.D., 2002. Flux versus decompression melting at stratovolcanoes in Southeastern Guatemala. J. Volcanol. Geotherm. Res. 119, 21–50.

Carn, S.A., Pyle, D.G., 2001. Petrology and geochemistry of the Lamongan volcanic field, East Java, Indonesia: primitive Sunda arc magmas in an extensional tectonic setting? J. Petrol. 42, 1643–1683.

Carr, M.J., 1984. Symmetrical and segmented variation of physical and geochemical characteristics of the Central American volcanic front. J. Volcanol. Geotherm. Res. 20, 231–252.

Carr, M.J., Mayfield, D.G., Walker, J.A., 1981. Relation of lava compositions to volcano size and structure in El Salvador. J. Volcanol. Geotherm. Res. 10, 35–48.

Castillo, P.R., Newhall, C.G., 2004. Geochemical constraints on possible subduction components in lavas of Mayon and Taal volcanoes, Southern Luzon, Philippines. J. Petrol. 45, 1089–1108.

Clavero, J.E., Sparks, R.S.J., Huppert, H.E., 2002. Geological constraints on the emplacement mechanism of the Parinacota debris avalanche, Northern Chile: Bull. Volcanology 64, 40–54.

Cotton, C.A., 1952. Volcanoes as Landscape Forms, 2nd ed. Whitcombe and Tombs, Christchurch, New Zealand.

Crippen, R.E., Hook, S.J., Fielding, E.J., 2007. Nighttime ASTER thermal imagery as an elevation surrogate for filling SRTM DEM voids. Geophys. Res. Lett. 34, L01302. doi:10.1029/2006GL028496.
Davidson, J., De Silva, S., 2000. Composite volcanoes. In: Sigurdsson, H., et al. (Ed.), Encyclopedia of Volcanoes. New York, Academic Press, pp. 663–681.
Dorendorf, F., Wiechert, U., Wörner, G., 2000. Hydrated sub-arc mantle: a source for the Kluchevskoy volcano, Kamchatka/Russia. Earth Planet. Sci. Lett. 175, 69–86.
Drake, R.E., 1976. Chronology of Cenozoic igneous and tectonic events in central Chilean Andes — latitudes 35°30′ to 36°S. J. Volcanol. Geotherm. Res. 1, 265–284.
Farr, T.G., et al., 2007. The shuttle radar topography mission. Rev. Geophys. 45, RG2004. doi:10.1029/2005RG000183.
Figueroa, O., Déruelle, B., Demaiffe, D., 2009. Genesis of adakite-like lavas of Licancabur volcano (Chile-Bolivia, Central Andes). Comptes Rendus Geoscience 341, 310–318.
Francis, P., 1993. Volcanoes: A Planetary Perspective. Oxford University Press, Oxford.
Garrison, G., Davidson, J., Reid, M., Turner, S., 2006. Source versus differentiation controls on U-series disequilibria: Insights from Cotopaxi Volcano, Ecuador. Earth Planet. Sci. Lett. 244, 548–565.
Grosse, P., van Wyk de Vries, B., Petrinovic, I., Euillades, P.A., Alvarado, G.E., 2009. Morphometry and evolution of arc volcanoes. Geology 37, 651–654. doi:10.1130/G25734A.1.
Hayakawa, Y.S., Oguchi, T., Lin, Z., 2008. Comparison of new and existing global digital elevation models: ASTER G-DEM and SRTM-3. Geophys. Res. Lett. 35, L17404. doi:10.1029/2008GL035036.
Hochstaedter, A.G., Kepezhinskas, P.K., Defant, M.J., 1996. Insights into the volcanic arc mantle wedge from magnesian lavas from the Kamchatka Arc. J. Geophys. Res. B101, 697–712.
Hora, J., Singer, B., Wörner, G., Beard, B.L., Jicha, B.R., Johnson, C.M., 2009. Shallow reservoir and deep crustal control on differentiation of calc-alkaline and tholeiitic magmas. Earth Planet. Sci. Lett. 28, 75–86.
Hubbard, B.E., Sheridan, M.F., Carrasco-Núñez, G., Díaz-Castellón, R., Rodríguez, S.R., 2007. Comparative lahar hazard mapping at Volcan Citlaltépetl, Mexico using SRTM, ASTER and DTED-1 digital topographic data. J. Volcanol. Geotherm. Res. 160, 99–124. doi:10.1016/j.jvolgeores.2006.09.005.
Huggel, C., Schneider, D., Julio Miranda, P., Delgado Granados, H., Kääb, A., 2008. Evaluation of ASTER and SRTM DEM data for lahar modeling: a case study on lahars from Popocatépetl Volcano, Mexico. J. Volcanol. Geotherm. Res. 170, 99–110. doi:10.1016/j.jvolgeores.2007.09.005.
Karátson, D., Thouret, J.-Cl., Moriya, I., Lomoschitz, A., 1999. Erosion calderas: origins, processes, structural and climatic control. Bull. Volcanol. 61, 174–193.
Katsui, Y., Oba, Y., Ando, S., Nishimura, S., Masuda, Y., Kurasawa, H., Fujimaki, H., 1978. Petrochmistry of Quaternary volcanic rocks of Hokkaido, North Japan. J. Fac. Sci. Hokkaido Univ. 4, Geol. Mineral. 18, 449–484.
Kepezhinskas, P., McDermott, F., Defant, M.J., Hochstaedter, A., Drummond, A.S., Hawkesworth, C.J., Kolloskov, A., Maury, R.C., Bellon, H., 1997. Trace element and Sr–Nd–Pb isotopic constraints on a three-component model of Kamchatka Arc petrogenesis. Geochim. Cosmochim. Acta 61 (3), 577–600.
Kersting, A.B., Arculus, R.J., 1994. Klyuchevskoy Volcano, Kamchatka, Russia; the role of high-flux recharged, tapped, and fractionated magma chamber(s) in the genesis of high-Al_2O_3 from high-MgO basalt. J. Petrol. 35, 1–41.
Leeman, W.P., Carr, M.J., Morris, J.D., 1994. Boron geochemistry of the Central American Volcanic Arc: constraints on the genesis of subduction-related magmas. Geochim. Cosmochim. Acta 58, 149–168.
Lyons, J.J., Waite, G.P., Rose, W.I., Chigna, G., 2009. Patterns in open vent, strombolian behavior at Fuego volcano, Guatemala, 2005–2007. Bull. Volcanol. doi:10.1007/s00445-009-0305-7.
Kervyn, M., Ernst, G.G.J., Goossens, R., Jacobs, P., 2008. Mapping volcano topography with remote sensing: ASTER vs SRTM. Int. J. Rem. Sens. 29, 6515–6538. doi:10.1080/01431160802167949.
Mamani, M., Wörner, G., Sempere, T., 2009. Geochemical variations in igneous rocks of the Central Andean Orocline (13° to 18°S): tracing crustal thickening and magma generation through time and space. Geol. Soc. Amer. Bull., B26538.1. doi:10.1130/B26538. irst published on September 25, 2009.
Masuda, I., 1979. Lateral variation of trace element contents in Quaternary volcanic rocks across Northeast Japan. Bull. Osaka Pref. Univ. 28, 105–125.
McNutt, S.R., Miller, T.P., Taber, J.J., 1991. Geological and seismological evidence of increased explosivity during the 1986 eruptions of Pavlof Volcano. Alaska. Bull. Volcanol. 53, 86–98.
McKnight, S.B., Williams, S.N., 1997. Old cinder cone or young composite volcano? The nature of Cerro Negro, Nicaragua. Geology 25, 339–342.
Milne, J., 1878. On the forms of volcanos. Geol. Mag. 5, 337–345 (Decade II).
Morrice, M.G., Jezek, P.A., Hart, S.R., Gill, J.B., Whitford, D.J., Monoarfa, M., 1983. An introduction to the Sangihe Arc: volcanism accompanying arc–arc collision in the Molucca Sea, Indonesia. J. Volcanol. Geotherm. Res. 19, 135–165.
Morris, J.D., Jezek, P.A., Hart, S.R., Gill, J.B., 1983. The Halmahera Island Arc, Molucca Sea collision zone, Indonesia: a geochemical survey. In: Hayes, D.E. (Ed.), The tectonic and geologic evolution of Southeast Asian seas and islands, part 2. AGU, Washington DC, pp. 373–387.
Nakagawa, M., 1992. Spatial variation in chemical composition of Pliocene and Quaternary volcanic rocks in Southwestern Hokkaido, Northeastern Japan Arc. J. Fac. Sci. Hokkaido Univ. 4, Geol. Mineral. 23, 175–197.
Neall, V.E., Stewart, R.B., Smith, I.E.M., 1986. History and petrology of the Taranaki volcanoes. Roy. Soc. New Zeal. Bull. 23, 251–263.
Nicholls, I.A., Whitford, D.J., 1976. Primary magmas associated with Quaternary volcanism in the western Sunda Arc, Indonesia. In: Johnson, R.W. (Ed.), Volcanism in Australasia. Elsevier, Amsterdam, pp. 77–90.
Ollier, C.D., 1988. Volcanoes. Blackwell, Oxford.
Ollier, C.D., Brown, M.J.F., 1971. Erosion of a young volcano in New Guinea. Z. Geomorphol. 15, 12–28.
Popolitov, E.I., Volynets, O.N., 1981. Geochemical Characteristics of Quaternary Volcanism of the Kurile–Kamchatka Island Arc and Some Problems of Petrogenesis. Nauka, Novosibirsk.
Portnyagin, M., Bindemann, I., Hoernle, K., Hauff, V., 2007. Geochemistry of primitive lavas of the Central Kamchatka Depression: magma generation at the edge of the Pacific Plate. In: Eichelberger, J., Gordeev, E., Kasahara, M., Izbekov, P., Lees, J. (Eds.), Volcanism and Subduction: The Kamchatka Region: Geophys. Monograph. Ser., 172. American Geophysical Union, Washington D.C, pp. 199–239.
Pyle, D.M., 1989. The thickness, volume and grainsize of tephra-fall deposits. Bull. Volcanol. 51, 1–15.
Rabus, B., Eineder, M., Roth, A., Bamler, R., 2003. The shuttle radar topography mission — a new class of digital elevation models acquired by spaceborne radar. J. Photogramm. Rem. Sens. 57, 241–262.
Ruxton, B.P., McDougall, I., 1967. Denudation rates in Northeast Papua from potassium–argon datings of lavas. Am. J. Sci. 265, 545–561.
Sobolev, A.V., Chaussidon, M., 1996. H_2O concentrations in primary melts from supra-subduction zones and mid-ocean ridges; implications for H_2O storage and recycling in the mantle. Earth Plan. Sci. Lett. 137, 45–55.
Stevens, N.F., Garbeil, H., Mouginis-Mark, P.J., 2004. NASA EOS Terra ASTER: volcanic topographic mapping and capability. Rem. Sens. Env. 90, 405–414. doi:10.1016/j.rse.2004.01.012.
Stewart, R.B., Price, R.C., Smith, I.E.M., 1996. Evolution of high-K arc magma, Egmont volcano, Taranaki, New Zealand: evidence from mineral chemistry. J. Volcanol. Geotherm. Res. 74, 275–295.
Stolz, A.J., Varne, R., Davies, G.R., Wheller, G.E., Foden, J.D., 1990. Magma source components in an arc–continent collision zone: the Flores–Lembata sector, Sunda Arc. Indonesia. Contrib. Mineral. Petrol. 105, 585–601.
Tolstikhin, I.N., Mamyrin, B.A., Khabarin, L.B., Erlikh, E.N., 1974. Isotope composition of helium in ultrabasic xenoliths from volcanic rocks of Kamchatka. Earth Planet. Sci. Lett. 22, 75–84.
Wheller, G.E., Varne, R., Foden, J.D., Abbott, M.J., 1987. Geochemistry of Quaternary volcanism in the Sunda–Banda Arc, Indonesia, and three-component genesis of island-arc basaltic magmas. J. Volcanol. Geotherm. Res. 32, 137–160.
Whitford, D.J., 1975. Strontium isotope studies of the volcanic rocks of the Sunda Arc, Indonesia, and their petrogenetic implications. Geochim. Cosmochim. Acta 39, 1287–1302.
Williams, H., McBirney, A.R., 1979. Volcanology. San Francisco, Freeman, Cooper and Co.
Wood, C.A., 1980. Morphometric evolution of cinder cones. J. Volcanol. Geotherm. Res. 7, 387–413.
Wörner, G., Harmon, R.S., Davidson, J., Moorbath, S., Turner, D., McMillan, N., Nye, C., Lopez-Escobar, L., Moreno, H., 1988. The Nevados de Payachata volcanic region (18°S/69°W, N. Chile): I. Geological, geochemical and isotopic observations. Bull. Volcanol. 50, 287–303.
Wörner, G., Hammerschmidt, K., Henjes-Kunst, F., Lezaun, J., Wilke, H., 2000. Geochronology (^{40}Ar–^{39}Ar-, K–Ar-, and He-exposure-) ages of Cenozoic magmatic rocks from Northern Chile (18°–22°S). Implications for magmatism and tectonic volution of the Central Andes. Rev. Geol. Chile 27, 205–240.
Wright, R., Garbeil, H., Baloga, S.M., Mouginis-Mark, P.J., 2006. An assessment of shuttle radar topography mission digital elevation data for studies of volcano morphology. Rem. Sens. Env. 105, 41–53. doi:10.1016/j.rse.2006.06.002.